Chapter 2

Growth of Quantum Confined Structures by Molecular Beam Epitaxy

RICHARD J. MATYI

Department of Materials Science and Engineering
University of Wisconsin—Madison
Madison, Wisconsin 53706

I. INTRODUCTION

The decade of the 1990s has begun with research and development on quantum well heterostructures that is growing at an astounding rate. Many of the developments in this area have been enabled by advances in the science and technology of advanced materials growth techniques such as molecular beam epitaxy (MBE). This chapter examines the advances that have been made in the MBE growth of III–V semiconductor struc-

Heterostructures and
Quantum Devices

tures that rely on quantum confinement for their operation. Although the basic science and technology of III–V MBE has been well covered in a number of review articles [1–4] and at least three excellent books [5–7], the factors that allow the existence of well-defined quantized energy states in small structures and the subsequent transport of electrons or holes through those states often place unique (and sometimes conflicting) constraints on the materials grower. Our focus will be on the MBE growth quantum wells and resonant tunneling structures (both two-terminal and three-terminal devices) in which quantum confinement is achieved in the growth direction. Although there has been significant progress in the MBE growth of quantum confined structures using silicon-based and II–VI MBE systems, we will concentrate solely on growth issues involving GaAs and other III–V materials.

II. MOLECULAR BEAM EPITAXY INSTRUMENTATION

MBE growth systems of the 1990s can still be represented by the schematic illustrations used in reviews of the technology that were published in the 1970s (see Fig. 1). That is, even the most advanced of MBE systems exhibits the following basic components:

- Sources for the molecular beams and mechanisms for controlling their fluxes
- An ultrahigh vacuum (UHV) growth chamber equipped with cryoshrouds
- Provisions for heating a substrate and maintaining it in a suitable geometry for growth
- Instrumentation for *in situ* characterization

These factors have been discussed at length in the books by Parker [6] and Herman and Sitter [7], and the excellent review by Chand discusses specific procedures for the growth of high-purity GaAs [8]. Advances in some specific aspects of MBE technology have had a positive impact in the growth of quantum structures, however, so a brief examination of these developments is in order.

A. Elemental Sources

The need for high-purity elemental sources for solid-source MBE has long been recognized. Because many phenomena in quantum well struc-

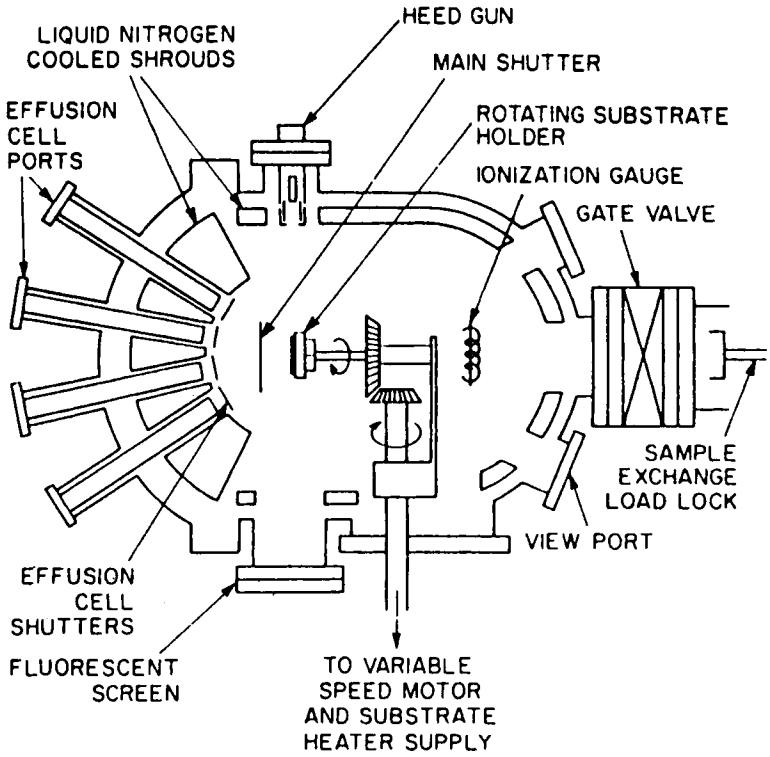

Fig. 1. Schematic illustration of a generic MBE system. (Adapted from Ref. 5.)

tures are extremely sensitive to trace impurities, the decrease in the background impurity levels in source materials has positively affected the MBE grower's capabilities.

1. Group III Sources

99.999999% pure (often described as "eight nines" or "8N") Ga is available from several vendors in the form of solid ingots. Seven nines (99.99999%) In is also now available. It is a welcome addition to the MBE grower's palette, because indium has generally been regarded as the "dirtiest" of the group III sources. Improved properties of In-containing layers have been observed by Scott *et al.* [9], who added a small amount of 6N aluminum to their indium source (~0.01 mol%). The affinity of aluminum for impurities was demonstrated by Tsang [3], who showed that oxygen impurities in aluminum are responsible for increases in the thresh-

old currents in GaAs/AlGaAs heterostructure lasers. Reduction of the concentration of dissolved oxygen in aluminum has required the use of zone refining under high-vacuum conditions, and this is now commercially available.

2. Group V Sources

Several vendors now supply seven nines As in charges that are shaped to fit specific effusion cells and crucibles; studies have demonstrated the superiority of shaped As charges over conventional "lump" arsenic [10]. Seven nines antimony is also readily available; however, use of this element in a conventional MBE system is often complicated by the tendency of Sb to condense at the cool opening of an effusion cell (see below). There are several problems associated with the use of phosphorus as an MBE source. The high vapor pressure of red phosphorus (10^{-3} torr at 150°C) at the temperatures used to bake a UHV deposition system means that it must be kept at a reduced temperature during system bakeout. Unfortunately, this means that residual gaseous impurities (notably H_2O) remain in the source. (The vapor pressure of the white allotrope is even higher.) Asahi *et al.* [11] have reported that the desorption of phosphorus from cryoshrouds as they warm up following growth can lead to extremely high pressures in the growth chamber. Fires have also occurred in phosphorus-containing MBE systems opened to air during maintenance.

3. Dopants

Extremely high-purity silicon for *n*-type doping is easily available, thanks to the silicon semiconductor industry's need for intrinsic high-resistivity Si for power and optoelectronic applications. It should be noted that silicon grown by the float-zone (FZ) method is significantly more pure than the Czochralski (CZ) silicon conventionally used for integrated circuit manufacture. It is not known how this difference might affect the performance of Si-doped quantum well structures. The situation with beryllium (the principal *p*-type dopant) is less favorable. Be is rarely found with purities exceeding 99.999%, so incorporation of contaminants would be expected in materials that are doped highly *p*-type. An alternative approach to *p*-type doping involves the use of elemental carbon. Although much of MBE technology has been developed with the thought that carbon incorporation into epitaxial layers is "bad," numerous studies have demonstrated that intentional carbon doping can yield very high hole concentrations with minimal adverse side effects [12].

B. Effusion Cell Technology

1. Conventional Effusion Cells

One difficulty with conventional effusion cells is that the molecular flux can exhibit variations with time. For instance, as an elemental source is depleted its surface area decreases and a higher cell temperature will be required to maintain a constant flux. Short-term variations also occur, such as the cooling of the effusion cell (and consequent decrease in beam pressure) immediately after the shutter is opened. Köhrbrück *et al.* [13] found that the thicknesses of GaAs quantum wells imbedded in AlGaAs barriers increased as the length of growth interruptions at the AlGaAs/GaAs interfaces increased. This effect was attributed to an increase in the temperature of the effusion cell when the shutter was closed, with the largest temperature increase (manifested by an enhanced growth rate and consequent thicker quantum well) occurring at the longest interruption time. Use of a specially designed crucible assembly has been found to minimize this problem [14].

2. High-Temperature Effusion Cells

A major limitation in conventional effusion cells occurs from the decomposition of the boron nitride crucible around 1300°C (typically indicated by the evolution of a nitrogen peak at mass 28 in a residual gas analyzer scan). Even without this limitation, radiative losses make it inadvisable to increase the temperature of a conventional effusion cell much higher because of the extremely high current that would be applied to the heater assembly and the concurrent (and equally unacceptable) heating of the effusion cell environment. Modifications to both the heater assembly and the heat shielding around the heater have permitted high-temperature effusion cells to attain temperatures of approximately 2000°C. Of course, boron nitride is not a suitable crucible material in this application; tungsten is used instead. Some questions may arise concerning the possibility of contamination of sensitive structures from metallic crucibles; a comparison of silicon doping performed using conventional and high-temperature cells with boron nitride and tungsten crucibles, respectively, does not seem to have been performed as yet. The principal use of high-temperature effusion cells arises in the deposition of new materials that were not previously compatible with conventional III–V growth systems [15].

3. Improved Group V Sources

The kinetic requirement of a V/III flux ratio greater than unity during growth requires a relatively large group V flux [16,17]. Because conven-

tional ion pumps are not efficient at removing group V molecules, the excess unincorporated flux results in the presence of a group V overpressure within the MBE chamber. Thus control of the group V environment at the growth surface is difficult at best. A further difficulty arises from the typical rapid depletion of the group V materials. A heavily used MBE system can experience significant downtime solely for the periodic recharging of the group V source material. Of course, the repeated exposure of the growth chamber interior to air is not beneficial to the subsequent deposition of impurity-sensitive quantum well structures. The high partial pressure that exists above the group V source material cell can lead to parasitic deposition at the entrance to the cell, where relatively cool surfaces (such as the aperture of the source flange cryoshroud) are present. In extreme cases the opening of the effusion cell can be completely closed off from such deposition.

Recent designs of group V effusion cells have overcome many of these difficulties. Their volumes are often significantly greater than those of typical group III effusion cells, thus increasing the lifetime of the source and minimizing up-to-air cycles. This simple approach is preferable to retractable effusion cells that can be isolated from the growth chamber by an isolation valve but suffer from mechanical and operational complexity. Parasitic deposition at the entrance of the effusion cell can be eliminated in effusion cells equipped with multiple heating zones to provide extra heat to the lip of the crucible.

As discussed later in Section III, early studies of MBE growth by Foxon and Joyce [16,17] demonstrated that major differences exist in the kinetics of incorporation of As_2 versus As_4. Since then a number of studies have demonstrated that dimeric arsenic provides a number of advantages. Kunzel and Ploog [18] reported that the use of As_2 eliminated the defect-induced bound exciton peak in photoluminescence spectra, and Neave *et al.* [19] reported a reduction in the concentration of deep traps when As_2 is used. The incorporation of both silicon [20] and carbon [21] is also significantly reduced by the use of As_2 versus As_4. Precise control of the group V flux has been demonstrated through the use of a "valved cracker," with control of the flux achieved by placing a mass flow control valve at the aperture of the cell [22,23]. Studies by Wicks and co-workers [24] have demonstrated that a valved phosphorus source can circumvent many of the difficulties typically associated with this element.

4. Resistively Heated Dopant Sources

Various groups have examined doping via resistive heating of an elemental filament of carbon [25] or silicon [26] for *p*-type and *n*-type doping,

respectively. The advantages of this approach include simplicity of cell design (and consequent low cost) and the elimination of nitrogen contamination from a boron nitride crucible at high temperatures. Although the conventional MBE practice of determining a doping calibration from a plot of carrier concentration versus the logarithm of the inverse absolute cell temperature cannot be applied with resistively heated sources, a study by King *et al.* [27] showed that a properly designed strip source can yield reproducible fluxes.

5. Electron Beam Sources

Electron beam (e-beam) evaporators have long been employed in silicon-based MBE systems, and the application of e-beam sources for Si-MBE is thoroughly reviewed in the literature [28]. The use of these sources in III–V growth systems has been far less widespread, despite the very promising work by Malik [29]. In Malik's system three e-beam sources were used to generate Ga, Al, and In molecular beams, with each source having its own flux monitor to provide feedback control. The dynamic feedback control resulted in unprecedented control of the molecular fluxes, giving the prospect of fabricating structures such as superlattices with sawtooth composition profiles and complex compositionally graded barriers.

C. Gas Sources

The replacement of conventional Knudsen effusion cells by sources employing gaseous precursors can made by replacing the group III sources, the group V sources, or both. Metalorganic MBE (MOMBE) derives the group III elements from the pyrolysis of metalorganic compounds (usually trimethyl or triethyl) on the heated substrate surface in the growth chamber while producing the group V elements from solid sources. On the other hand, gas source MBE (GSMBE) produces the group III elemental fluxes from sources in conventional effusion cells while the group V elements are derived from AsH_3 or PH_3. Chemical beam epitaxy (CBE) replaces both group III and group V effusion cells with gaseous sources.

With the extensive use of group V hydrides as well as triethyl and trimethyl group III compounds such as TEGa, TEIn, and TMAl, CBE and its derivatives are reminiscent of metalorganic chemical vapor deposition (MOCVD), albeit performed in what is nominally a UHV environment (although typical pressures during film deposition are significantly higher than those observed under an arsenic overpressure during solid-source

MBE growth). The vacuum conditions employed in CBE, GSMBE, and MOMBE permit the application of *in situ* analytical techniques to the growth process. The use of gas sources removes the need for periodic replacement of solid-source materials, thus offering the prospect of moving MBE from a batch-processing to a continuous-processing mode of operation. The availability of PH_3 as a phosphorus source represents a significant advantage of this technique, because of the problems associated with solid-source phosphorus growth mentioned earlier. However, CBE and the other gas source techniques also have their problems. The high gas loads that accompany growth from gas sources often require a major augmentation to the typical MBE vacuum system. The decomposition of organometallic Group III compounds leads to unintentional carbon incorporation and thus increases the background doping level of materials grown with gas sources. Finally, the use of AsH_3 and PH_3 (both of which must be handled as gases in high-pressure cylinders) requires much more stringent safety requirements than are usually needed for solid-source MBE. Tsang [30] has presented a thorough review of CBE in an earlier volume of this series, and the reader is referred to that treatment for a discussion of gas source epitaxial growth.

D. Ultrahigh Vacuum Technology

1. Vacuum Pumps

Ion pumps, cryopumps, and titanium sublimation pumps remain the primary pumping systems for MBE systems. Although sublimation pumps are not very useful for pumping arsenic from a III–V MBE system, they are efficient at removing contaminants such as surface oxides as well as species that desorb from hot filaments (such as effusion cells and substrate heaters). Sublimators should not be run during a critical portion of a growth run (i.e., in the middle of a quantum well), because oxygen outgassed from the sublimator filament may become incorporated in the growing layer. Instead, it is useful to operate a sublimation pump immediately prior to growth, so that an active gettering layer of titanium can be available throughout the run. There is anecdotal evidence that by partially coating the interior of the growth chamber with the flux from the Al source, a reactive pumping surface is created that improves the quality of quantum well structures [31].

The addition of gaseous sources alters the vacuum requirements of MBE. Typical CBE systems utilize large-capacity turbomolecular or diffusion pumps to handle the large gas loads that accompany the use of gas

sources. Of course, due to the toxic nature of the group V hydrides, CBE pumping systems must also include the proper safety equipment.

2. Cryoshrouding

An important early advance in MBE technology was the addition of liquid nitrogen (l-N_2) cryoshrouds along the walls of the growth chamber and around the effusion cell sources. Cryoshrouding provides extra pumping capability for arsenic and phosphorus (elements with a low pumping speed with conventional ion pumps), while the presence of a cold surface is highly effective at trapping impurities and contaminants that are desorbed from substrate heaters and effusion cells during the growth process. Some MBE systems utilize an l-N_2–cooled panel with a substrate heater inside a preparation chamber that is immediately adjacent to the main growth chamber. This allows the substrate and its mounting block to be partially thermally cleaned prior to insertion into the UHV growth environment, thus reducing contamination of the growth chamber.

One of the problems with l-N_2 cryoshrouding is the high boil-off rate of the liquid nitrogen. This is especially severe with the shroud surrounding the elemental sources, since the close proximity of hot effusion cells represents a severe radiant thermal load. Various laboratories have successfully employed a cooling system with a recirculating, refrigerated mixture of water with ethylene glycol maintained at $-5°$ to $-20°C$ to cool the source shroud, with liquid nitrogen being used only to cool the chamber panels. This approach maintains an l-N_2 surface in the chamber near the sample to provide some cryopumping; however, it reduces the grievous boil-off rate caused by the proximity of the effusion cells operating at high temperature. There do not appear to be any comparative studies of the optical or electrical characteristics of a test structure grown from the same system using the two different source shroud cooling methods.

3. The Final Frontier

An alternative method for maintaining a UHV environment for epitaxial growth could involve performing MBE in outer space [32,33]. In this approach, a "vacuum wake shield" would be carried by the space shuttle, and effusion cells and a substrate heater would be positioned behind the shield. Calculations indicate that the vacuum on the "leeward" side of the shield should be several orders of magnitude superior to those obtainable on Earth (10^{-14} and 10^{-18} torr for hydrogen and oxygen, respectively [32,33]), leading to the prospect that electronic device structures grown in

space would exhibit properties superior to those attainable in terrestrial MBE growth (although charged particle fluxes during times of enhanced geomagnetic activity could produce undesirable levels of radiation damage [34]). It is not clear whether the improvements in the performance of a structure such as a resonant tunneling diode would be justified by the efforts required to grow that structure in space.

E. Substrate Issues: Preparation and Heating

It is well known in the MBE community that substrate preparation is one of the principal limiting factors in successful epitaxial growth. There are several "recipes" for the preparation of III–V substrates for MBE growth; in particular, Tsang [3] gives a detailed enumeration of the steps necessary for substrate preparation. The purpose of these chemical treatments is to remove both residual polish damage and prior contamination (notably carbon and metals) from the substrate surface by chemical etching and to encourage the growth of a native oxide that is easily desorbed immediately prior to growth. Unfortunately, experience has suggested that the same recipe can rarely be reproduced exactly when translated from one laboratory to the next. Simple procedures such as "blow dry with nitrogen" will be executed with different results in different locations, and the result of this variance is often reflected in the structure and properties of the final epitaxial layer.

An important (and welcome) change in this state of affairs has been the advent of GaAs substrates that require no chemical treatment by the MBE grower. These so-called epi-ready substrates have already been subjected to the chemical treatments needed to remove damage and contamination; moreover, they have been treated in such a way as to have a relatively stable (but easily desorbed) native oxide. Although the vendors of these wafers are typically reluctant to reveal the procedures used to achieve this collection of desirable properties, it is likely that processes similar to those described by Ploog [35] are employed. The suppliers' claim that these substrates can be inserted directly into the MBE growth chamber appears to be valid, as epi-ready wafers are now being used at a number of locations. Surprisingly, epi-ready substrates are only slightly more expensive than conventional GaAs wafers. At this writing, only GaAs substrates are available; users of InP or GaSb have no choice but to perform the conventional wafer preparation procedures.

Before growth, the prepared substrate is either mounted onto a molybdenum block with indium solder or inserted into a full wafer, indium-free sample holder. The choice of indium-bonded or indium-free mounting is

often determined by economics—well-funded installations where structures are being grown for large-scale device fabrication invariably utilize indium-free mounting, while smaller laboratories can extend the number of growth runs per 2-inch substrate by indium mounting small cleaved pieces. There is some evidence that cross-doping or contamination from indium solder can degrade device performance, however [36]. The mounted substrate can then be inserted into the growth chamber and heated under a group V flux until the surface oxide is desorbed and a clear reconstruction pattern is observed with reflection high-energy electron diffraction (RHEED). The time, temperature, and group V flux used to produce a clean, reconstructed surface vary from one laboratory to another.

The subject of temperature measurement has been addressed by a number of investigators, because the use of a rotating sample block or indium-free mounting (or both) precludes good contact between a control thermocouple and the substrate. Optical pyrometry is thus widely used for MBE temperature measurement. Silicon-doped GaAs is relatively opaque to infrared radiation; however, due to the temperature dependence of the GaAs bandgap [37], undoped GaAs is relatively transparent to infrared radiation at low temperatures but becomes absorbing over an increasing range of wavelengths as the temperature is increased. Thus a short-wavelength pyrometer (0.8 to 1.1 μm) is necessary for accurate temperature measurements [38]. Many of the issues concerning the use of optical pyrometers for III–V MBE have been examined by Wright and co-workers [39], who have reported a reliable calibration procedure. The use of RHEED to determine the surface temperature via the transition from a gallium-rich to an arsenic-rich reconstruction under (perfect vacuum) Langmuir conditions has also been demonstrated [40]. *In situ* monitoring of GaAs photoluminescence has been shown to be effective for the measurement of low (25 to 450°C) substrate temperatures [41].

Once the substrate surface has been prepared and the proper temperature has been achieved, growth can proceed. It will become evident in the following discussion that the fabrication of materials for quantum confinement places severe demands on the MBE grower with regard to vacuum integrity and both flux and temperature stability. An accurate knowledge of deposition rates, alloy compositions, and doping levels is essential for the successful growth of these structures. Although the first two of these can (and should) be monitored using oscillations in the intensity of features in the RHEED pattern during growth, control of doping can be achieved only through frequent *ex situ* calibrations of test structures with capacitance–voltage (C–V) profiling or similar techniques. The reader is strongly urged to consult reviews that give detailed information on the

operational aspects of MBE growth [7,8]; however, it should be remembered that each MBE installation is unique and that modifications to published procedures are likely to be necessary.

III. PROPERTIES OF RESONANT TUNNELING DIODES

A. AlGaAs/GaAs

Soon after the prediction in 1973 by Tsu and Esaki [42] that the current through a tunneling barrier should go through a maximum when the injected carriers achieve certain resonant energies, Chang *et al.* [43] fabricated the first MBE-grown structure that exhibited evidence of negative differential resistance (NDR). There was little further activity in this area until 1983, when Sollner and co-workers reported the observation of room-temperature resonant tunneling [44] and low-temperature microwave oscillations up to 2.5 THz [45] in an AlGaAs/GaAs double-barrier structure. About the same time, NDR in resonant tunneling structures grown by MBE was reported by Shewchuk *et al.* [46] and Tsuchiya and Sakaki *et al.* [46].

Figure 2 illustrates schematically a typical *n*-type resonant tunneling structure, commonly called a resonant tunneling diode (RTD), where a GaAs quantum well is clad by two thin barrier layers of a material with a larger bandgap (e.g., AlGaAs). In this case the contact layers are doped *n*-type (for electron tunneling devices); tunneling is achieved when the structure is biased so that the Fermi level of one contact aligns with a quantized energy level in the well. Undoped "spacer" layers are often inserted on the outbound sides of the barrier layers, ostensibly to reduce the diffusion of dopants into the tunneling heterostructure.

One of the principal gauges of the effectiveness of an RTD is the ratio of two currents: the maximum current observed when the energy of the injected carriers is in resonance with an energy level in a quantum well and the minimum current that exists when the injected carrier energy is sufficiently increased to destroy the resonance. This "peak-to-valley" ratio (PVR) in the current–voltage (I–V) characteristics of a double-barrier structure is sensitive to the relative magnitudes of a number of resonant, nonresonant, and parasitic currents. Some of the major contributions to the overall carrier transport in a double-barrier structure include [48] (a) resonant tunneling, (b) tunneling through a higher resonance level, (c) thermionic emission, (d) field-assisted tunneling, (e) tunneling through evanescent states, (f) inelastic tunneling, and (g) surface leakage current. These processes are illustrated in Fig. 3.

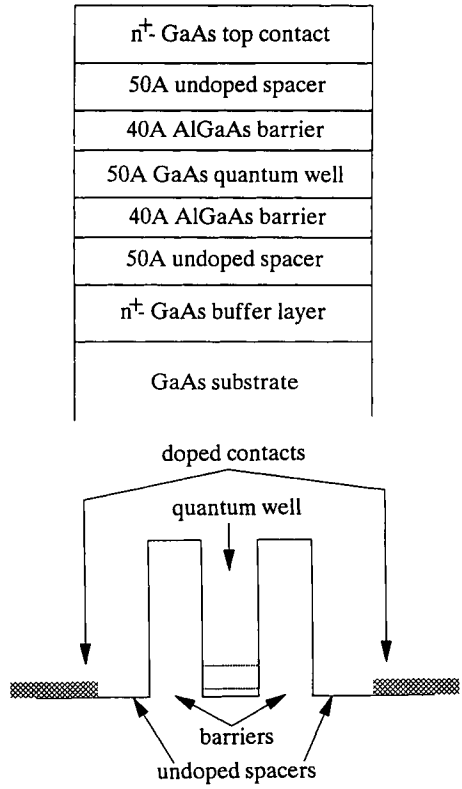

Fig. 2. Schematic illustration of the MBE-grown structure and the corresponding conduction band diagram for a typical *n*-type resonant tunneling structure in which a 50-Å GaAs quantum well is clad by two 40-Å AlGaAs barrier layers and 50-Å undoped GaAs spacer layers.

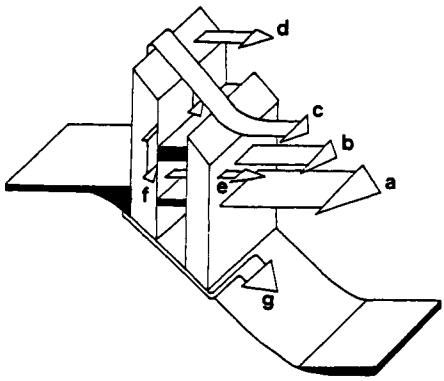

Fig. 3. Contributions to the resonant and nonresonant currents in a tunneling diode: (a) resonant tunneling; (b) tunneling through a higher resonance level; (c) thermionic emission; (d) field-assisted tunneling; (e) tunneling through evanescent states; (f) inelastic tunneling; and (g) surface leakage current. (From Ref. 48.)

The process of achieving a high peak-to-valley ratio is thus an exercise in enhancing the resonant tunneling peak current density while minimizing all nonresonant contributions to the valley current. Although many of these contributions can be altered through changes in the design of the structure, a number of factors that modify both resonant and nonresonant current are due solely to specific MBE growth conditions. The interfacial roughness of the quantum well is one obvious contributor to the performance of an RTD. Theoretical studies by Ping and Jiang [49] have shown that interfacial roughness results in fluctuations in the thicknesses of both the quantum well and the barriers, leading to oscillations about, and a reduction in, the peak current. This is undesirable, since a high current density is desirable to reduce the *RC* constant and increase the operating speed of the device. Liu has found (again by a theoretical approach) that scattering from interfacial roughness broadens the resonance and decreases the resonant tunneling peak current [50,51]. This agrees with the observation that scattering from remote impurities and interface roughness contributes to relaxation of electron momentum, thus decreasing negative differential conductivity and drift velocity at high fields [52].

Ideally, then, one would like to measure quantitatively the degree of interfacial roughness in an RTD and relate it to the observed transport characteristics of the device. Epitaxial film growers often justify their craft by claiming they can control growth one atomic layer at a time. If this were indeed the case, the interfaces between grown layers would be uncontaminated, perfectly smooth, and perfectly abrupt. Unfortunately, this goal is never achieved in practice, a matter that is of no small consequence to the device physicist, who typically models a structure by assuming ideal interfaces. A comprehensive treatment by Herman *et al.* [53] has covered this subject in depth; the reader is encouraged to consult this work for a more through examination of epitaxial semiconductor interfaces.

Unfortunately, the "standard" quantum well characterization technique—the observation of the excitonic spectrum using photoluminescence—is not possible in resonant tunneling structures, because the doping that is required in the top and bottom electrical contacts effectively masks the PL emission from the energy levels in the quantum well [54]. Also, as mentioned earlier, the length scale over which roughness is measured in a PL experiment may not be particularly meaningful in terms of electron transport. The most sensitive characterization tool for the analysis of the structure of materials used in resonant tunneling applications appears to be the tunneling device itself.

An early investigation of the effects of MBE growth conditions on the performance of AlGaAs/GaAs RTDs was reported by Lee and Reed [55].

This work demonstrated that the use of low growth rates for both the GaAs and AlGaAs ($x_{Al} \approx 0.3$) layers along with the use of an elevated substrate temperature (640° versus 600°C) was beneficial in producing structures that exhibited NDR at room temperature. Further improvement in the NDR characteristics was achieved when the silicon doping of the *n*-GaAs top and bottom contact layers was graded from 2×10^{18} to 2×10^{16} cm^{-3} within 300 to 500 Å of the AlGaAs barriers and 20- to 50-Å undoped GaAs spacers were inserted immediately adjacent to the barriers. PVRs of 1.75 : 1 and 7 : 1 were reported for the improved structure at room temperature and 77 K, respectively [55]. Significantly higher peak-to-valley ratios were reported by Goodhue *et al.* [56], who fabricated resonant tunneling structures using pure AlAs barriers. They observed a PVR of 3.5 : 1 (10 : 1) at room temperature (77 K) in a structure with 15-Å barriers and a 45-Å well. The entire structure was grown at the relatively low temperature of 560°C.

Huang *et al.* [57] have systematically modified a symmetric RTD consisting of a 50-Å GaAs quantum well, 50-Å AlGaAs barriers ($x_{Al} = 0.3$), 25-Å undoped GaAs spacers, 500-Å lightly doped *n*-GaAs (2×10^{16} cm^{-3}), and 0.5-μm (1.0-μm) top (bottom) heavily doped *n*-GaAs (2×10^{18} cm^{-3}) contact layers. This baseline structure typically exhibited a room-temperature peak-to-valley ratio of 1.85 : 1. An enhanced PVR of 2.1 : 1 (7.0 : 1) at room temperature (77 K) was achieved when the contact was graded to 2×10^{14} cm^{-3} prior to the undoped spacer. Further improvements were achieved when the aluminum content of the barriers was increased to $x = 0.42$, which increased the room temperature (77 K) PVR to 3.6 : 1 (13.5 : 1).

In the preceding discussion "typical" values of the PVR were cited, in contrast to the natural desire to report the "best" value. Variations across a large substrate should be expected because of both random defects generated during MBE growth and systematic changes that could arise (for instance) from nonuniform flux distributions from effusion cells or from radial variations in substrate temperature caused by the substrate heater. This issue has been examined quantitatively by Reed and coworkers [58], who characterized the variations in the widths of both the barriers and the quantum well in an AlGaAs/GaAs RTD across an MBE-grown wafer. The tunneling current density through a barrier of average height V and thickness d can be estimated from

$$J(V) = \frac{2\pi E v}{d^2 \hbar} e^{-2d\sqrt{2m^* V/\hbar}},$$

where m^* is the effective mass of the electron in the barrier and $\hbar$ is Planck's constant [59]. Figure 4 (top) shows a map of AlGaAs tunnel

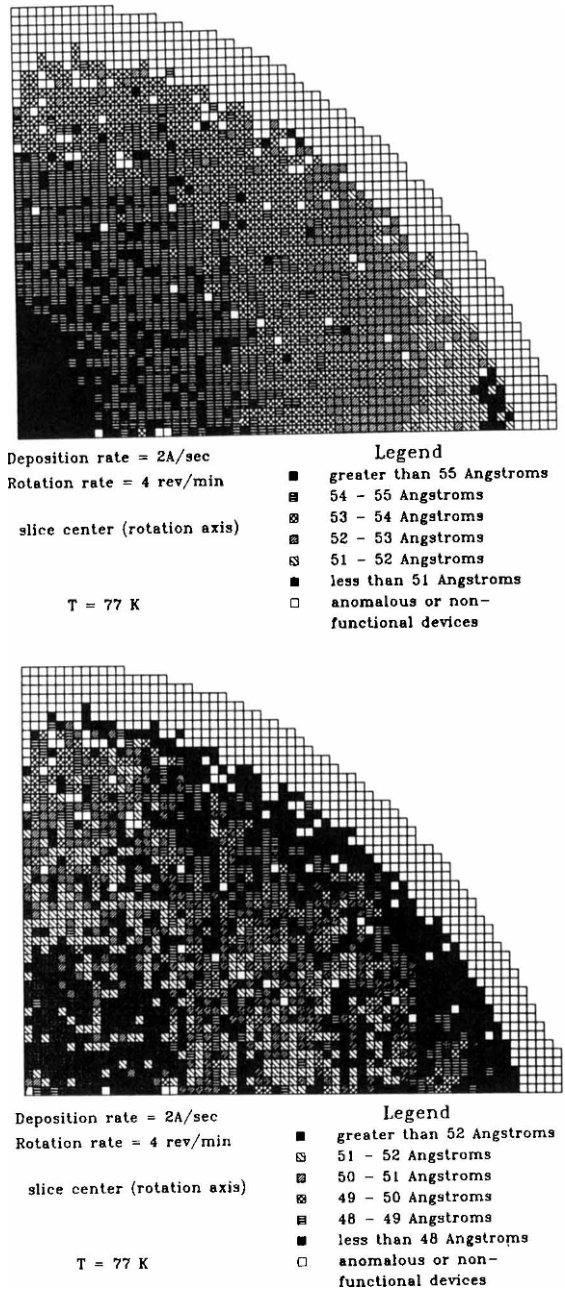

Fig. 4. Maps of (top) the AlGaAs tunnel barrier width and (bottom) GaAs quantum well width across one-quarter of a 2-inch substrate. (From Ref. 58.)

barrier widths across one quarter of a 2-inch substrate where the nominal (design) barrier width was 50 Å. The figure indicates the presence of growth rings and axial asymmetry; these features were attributed to the finite shutter open time and the fact that the ratio of the deposition time and the substrate rotation period was not integral [58]. Similarly, Fig. 4 (bottom) illustrates the spatial variations in the quantum well width determined from the voltage at which the NDR occurred. The figure demonstrates that the quantum well widths are less well defined than the tunnel barrier contours; in addition, the well widths do not exhibit the axial asymmetry. These data suggest that the width of the quantum well in a double-barrier structure is more "stable" than the barrier widths.

Another result of the study by Huang *et al.* was the finding that RTD structures grown on semi-insulating (SI) substrates were superior (in terms of PVR) to nominally identical structures grown on semiconductive (SC) Si-doped substrates. There are several possible reasons for this. The least likely of these is that silicon will diffuse from the substrate into the growing layer during film deposition, thus increasing the background doping in structures grown on SC substrates. An equally tenuous possibility arises from the unofficial reputation of Si-doped GaAs as being "dirtier" than SI wafers, with an increase in the background doping arising from desorbed species in the substrate. A more plausible explanation for the difference between the two substrates is the previously mentioned effect of doping on the infrared transmission characteristics of GaAs [37]. Different effective substrate temperatures could have several effects, such as altering the composition of the AlGaAs barriers, changing the degree of interfacial smoothness, and affecting the activation of (intentional) Si doping in the device structure. Campbell *et al.* [60] examined the effect of substrate temperature on GaAs/AlAs RTDs and found that while the peak-to-valley ratio did not change significantly between samples grown at 550, 600 and 650°C, the deep-level trap concentrations were substantially lower in samples grown at the highest (650°C) temperature.

The design of the barriers has received a great deal of attention because of the accessibility of this parameter to the MBE grower. Huang *et al.* [57] reported an increase in PVR from 2.1 : 1 to 3.6 : 1 as the aluminum concentration was increased from 30% to 42%. A subsequent study by Söderström and Anderson [61] illustrated the effects of the barrier on the transport properties in an MBE-grown AlGaAs/GaAs RTD. Figure 5 shows the effect of the thickness of pure AlAs barriers and the effect of aluminum concentration for fixed barrier thickness in an RTD with a 45-Å quantum well and typical doping and spacer layers [61]. Guéret and co-workers [62,63] varied the thickness of AlGaAs barriers ($x_{Al} = 0.14$) around a 70-Å GaAs well and found that the peak current scaled well with the transmis-

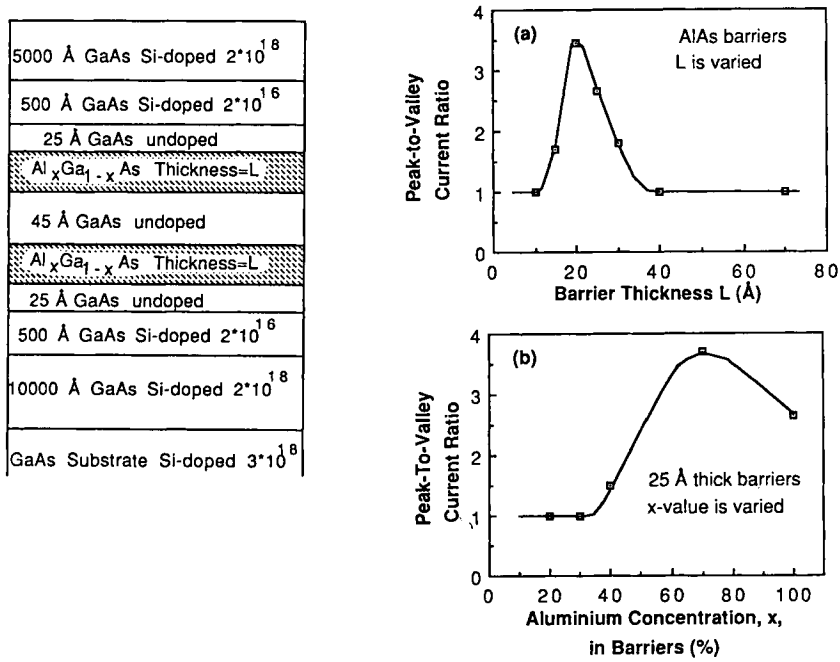

Fig. 5. Effect of the thickness of pure AlAs barriers and effect of the aluminum concentration for fixed barrier thickness in an RTD with a 45-Å quantum well and typical doping and spacer layers. (From Ref. 61.)

sion coefficients of the tunnel barriers. This indicated that the main source of momentum nonconservation (or nonresonant valley current) is interfacial roughness. Remote impurity scattering in the Si-doped GaAs contacts, phonon scattering, and barrier alloy scattering were all found to be negligible with respect to interfacial roughness scattering [63].

In order to increase the PVR of a double barrier structure, it might be better to lower the valley current than to raise the peak current. This was the approach taken by Cheng and Harris [64], who introduced a "chair barrier" consisting of a thin (four-monolayer) undoped AlGaAs layer ($x_{Al} = 0.14$) on the undoped spacer side of one AlAs barrier in an AlAs/GaAs RTD. Under forward bias conditions, where electrons encounter the chair barrier before the first tunnel barrier, the average PVR was 5.0 : 1 at room temperature, a remarkable increase over the typical value of 4.1 : 1 (by itself an excellent result) for a similar structure fabricated without the chair barrier. This is not the only approach that can be taken, since Riechert *et al.* [65] have reported that the insertion of a "prewell"

consisting of 40 Å of undoped $In_{0.15}Ga_{0.85}As$ increased the typical PVR of a 40-Å $Al_{0.6}Ga_{0.4}As$/30-Å GaAs double-barrier structure from 4.5 : 1 (without InGaAs prewell) to 5.7 : 1 (with prewell). In addition to causing a dramatic improvement in the PVR, the insertion of the InGaAs prewell more than doubled the peak current from 7×10^3 A/cm^2 (without prewell) to 1.7×10^4 A/cm^2 (with prewell). Similar results have been obtained by Wie and Choi [66] when an InGaAs prewell was inserted on the emitter side of an AlAs/GaAs RTD.

An alternative approach to AlGaAs barriers involves the use of AlAs/GaAs superlattice barriers. By replacing the AlGaAs barriers with 2.5 periods of 8-Å AlAs/8-Å GaAs in which brief (2-second) growth interruptions were introduced at each interface, Reed *et al.* [67] observed a slight improvement in the room temperature peak-to-valley ratio (1.8 : 1 vs. 1.75 : 1). Much greater improvement was found by Huang *et al.* [57], who reported a typical PVR with a binary superlattice barrier of 3.0 : 1 (compared with 1.85 : 1 for the same structure with alloy barriers); ratios as high as 3.9 : 1 (21.7 : 1) were observed at room temperature (77 K). No growth interruptions were reported in this case. Later work by Paulus *et al.* [68] in which the barriers consist of 3.5 periods of 8.5-Å AlAs/8.5-Å GaAs yielded a room-temperature PVR of 5.4 : 1.

The use of superlattice barriers offers the prospect of varying the height of the barrier by altering the superlattice period. Sen and co-workers [69] have exploited this capability by fabricating double-barrier *parabolic* quantum well structures with short-period GaAs/AlGaAs superlattices [60]. (Strictly speaking, such structures should be termed *quasiparabolic* because the well is formed by a superlattice instead of continuous composition grading [70].) In one case a 300-Å parabolic well was bounded by a 20-Å AlAs barrier, while the effective aluminum composition inside the well was graded from $x = 1$ at the edges to $x = 0$ at the center. This was accomplished by varying the duty cycle of the Al-rich layer in an AlGaAs/GaAs superlattice: the portion of the well from $x = 1$ to $x = 0.49$ was achieved using an AlAs/GaAs superlattice, while the range $0.49 \leq x \leq 0$ was grown by means of an $Al_{0.5}Ga_{0.5}As$/GaAs superlattice. The I–V characteristics at 7.4 K exhibited inflections that were regularly spaced in voltage (in contrast with the conventional square well, where the energy levels are quadratically spaced). Chou and Harris [70] fabricated a similar parabolic quantum well structure consisting of 30-Å AlAs barriers and a 315-Å quantum well formed using a 21-period $Al_{0.3}Ga_{0.3}As$/GaAs superlattice. The effective composition grading was again achieved by varying the thickness of the AlGaAs layer in each 15-Å-thick period, with the thickness of the AlGaAs layers increasing quadratically from the center of the well. At room temperature equally spaced resonant tunneling transitions

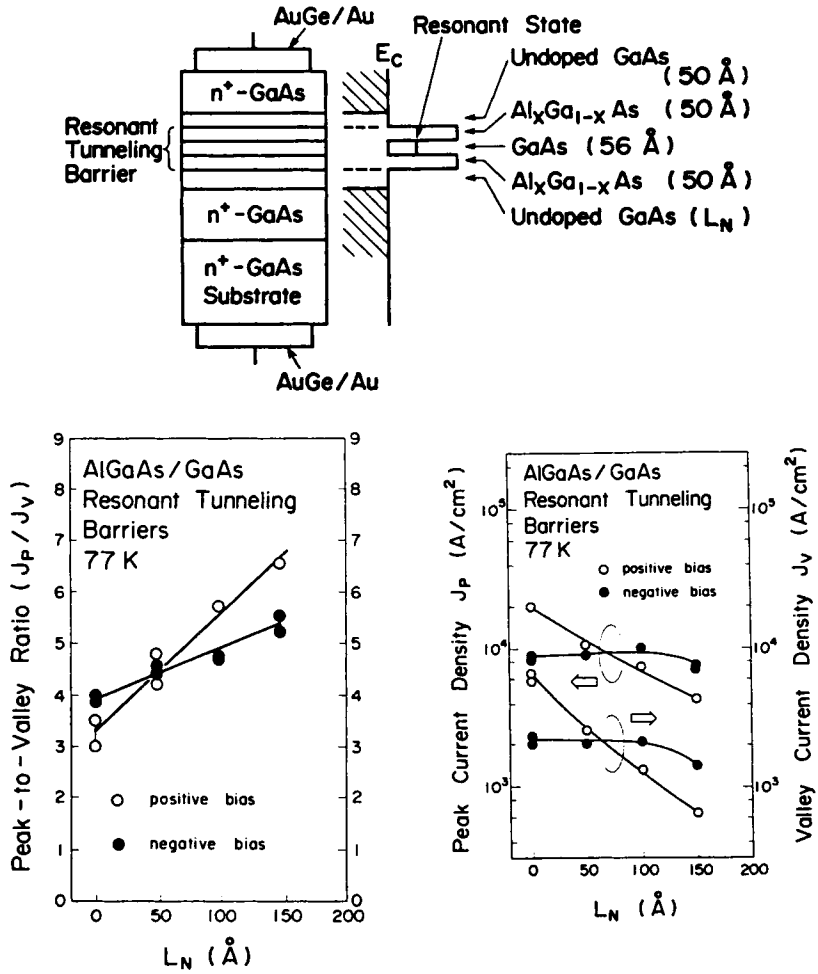

Fig. 6. Structure schematic of an AlGaAs/GaAs RTD (x_{Al} = 0.33) grown at 580°C by MBE, along with the effect of one undoped spacer on the PVR and current density characteristics. (From Ref. 71.)

were observed, and NDR was seen at 77 K, with the largest PVR being 1.4 : 1.

Doping methods will also have a significant impact on a structure's NDR characteristics. A particularly elegant study of the effect of (undoped) spacer thickness was that made by Muto and co-workers [71]. Figure 6 illustrates the structure schematic of an AlGaAs/GaAs RTD (x_{Al} = 0.33) grown at 580°C by MBE, along with the effect of one undoped

spacer on the PVR and current density characteristics. Significant improvements in the peak-to-valley ratio with increasing spacer layer thickness are seen, particularly in the case of positive bias (where the electrons encounter the variable spacer before the first tunnel barrier). No definitive mechanism for the increase in the PVR with increasing spacer layer thickness was given, although ionized impurity scattering and band bending from the high electron concentration in the quantum well at high peak current densities are possible [71].

The effects of spacer layer thickness on RTD I–V characteristics has been examined by Yoo *et al.* [72]. Whereas they initially observed an increase in the PVR with increasing spacer thickness in AlGaAs/GaAs double-barrier structures, Yoo *et al.* found that the PVR began to decrease at large thicknesses ($\geq$1000 Å). They attributed this to the fact that the presence of a thick spacer leads to the formation of an emitter spacer barrier; in the thick spacer case, thermionic emission over this barrier becomes the rate-limiting transport process [72]. This reduces the peak current, thus reducing the overall PVR. This mechanism is similar to the predictions of Mehdi and co-workers [73] that the junction potential at the n^+–i contact–spacer junction raises the potential of the double-barrier region [73].

The decrease in peak current density with increasing spacer layer thickness is a troublesome aspect of RTD design. Yang and Matyi [74] reported a double-barrier structure that exhibited a peak current density of 1.32×10^5 A/cm^2, a value comparable to that of a bipolar transistor. They also found that doping of the AlGaAs barriers ($x_{Al} = 0.4$) with silicon to 2×10^{18} cm^{-3} decreased, but did not eliminate, NDR at 77 K. The effects of n-type doped AlAs barriers have subsequently been examined by Cheng and Harris [75], who observed room temperature NDR with a peak-to-valley ratio of 2.7 : 1 at a doping level as high as 3×10^{18} cm^{-3}. Wolak and co-workers [76] have developed a coherent transport model to design GaAs/AlAs RTDs that exhibit peak current densities of 2.5×10^5 A/cm^2 at room temperature.

B. AlGaAs/InGaAs/GaAs

In a conventional AlGaAs/GaAs resonant tunneling structure, control of the voltage at which the peak current occurs can be accomplished only by varying the thickness of the quantum well; a thinner well is desirable to retain electron wave coherence in order to maximize the PVR. Because both peak current voltage control and a large PVR are useful for device applications, an independent method for varying the energy levels in the

quantum well is desirable. One way to accomplish this is to add indium to the well, since the bandgap of $In_xGa_{1-x}As$ decreases with increasing indium content. Toyoshima *et al.* [77] fabricated RTDs consisting of 30-Å AlAs barriers and 70-Å quantum wells of either GaAs or $In_{0.1}Ga_{0.9}As$ grown at 600°C. They observed NDR at room temperature with a PVR of about 1.3 : 1 in both cases; at 77 K the PVR of the sample with an In well was slightly superior to that obtained from the AlAs/GaAs structure (13 : 1 vs. 10 : 1). As expected, addition of indium to the quantum well lowered the voltage corresponding to the peak current.

Concurrently with the above work, Reed and Lee [55,78] fabricated a double-barrier structure consisting of 40-Å $Al_{0.25}Ga_{0.75}As$ barriers and a 60-Å $In_{0.2}Ga_{0.8}As$ quantum well. During the MBE growth the substrate temperature was lowered to 550°C for the InGaAs well in order to inhibit indium desorption. The 77-K PVR in this structure was 2.6 : 1, but at room temperature NDR vanished. At this high indium content the quantum well ground state was "hidden" below the Fermi level of the injector; tunneling occurred via the first excited state in the well [78]. A low substrate temperature (550°C) was also used by Yang and Shih [79] to grow an RTD with 30-Å $Al_{0.35}Ga_{0.65}As$ barriers and an $In_{0.2}Ga_{0.8}As$ well. Despite the fact that the AlGaAs was grown at such a low temperature, a 77-K PVR of 6 : 1 was demonstrated. Yang and Shih attributed this to the incorporation of indium into the AlGaAs. Unfortunately, the substrate temperature was not reported by Söderström *et al.* [80], who observed a 77-K PVR of 3 : 1 in a structure consisting of a 50-Å $In_{0.08}Ga_{0.92}As$ quantum well with 50-Å $Al_{0.25}Ga_{0.75}As$ barriers.

Although in none of these cases is there any indication of misfit dislocation generation (since the leakage currents associated with dislocations would probably eliminate any evidence of NDR), the device characteristics reported are decidedly inferior to those illustrated by Toyoshima *et al.* The reasons for this are not clear; possible causes include differences in indium sources (again, indium is traditionally regarded as the least pure of the group III sources), alloy segregation in the InGaAs quantum wells, and differences in substrate temperatures (not reported by Söderström *et al.*) or growth rates (not reported by Söderström *et al.*, Yang and Shih, or Toyoshima *et al.*).

Recent attempts to fabricate RTDs with InGaAs quantum wells have been more successful in producing structures with high PVR values. For instance, a series of InGaAs/AlAs/GaAs structures has been described by Kapre and co-workers [81]. These were grown at a fixed temperature of 580°C with all GaAs, AlAs, and InGaAs layers being grown at 4, 2, and 3.6 seconds per monolayer, respectively (one monolayer equals 2.8 Å). Kapre *et al.* reported a room temperature PVR of 2 : 1 for a sample con-

sisting of a 54-Å $In_{0.1}Ga_{0.9}As$ well that was clad with 28-Å AlAs barriers and 51-Å GaAs undoped spacer layers. Increasing the well thickness to 71 Å (still well below the critical thickness for misfit dislocation formation [82]) decreased the room temperature PVR to 1.2 : 1; however, replacement of the undoped GaAs spacers with undoped $In_{0.1}Ga_{0.9}As$ of the same thickness increased the PVR to 3.2 : 1. This value was eclipsed by Riechert and co-workers, who reported a typical room-temperature PVR of 3.95 : 1 for an $Al_{0.6}Ga_{0.4}As$ barrier/$In_{0.08}Ga_{0.92}As$ well structure with undoped GaAs spacers. Not to be outdone, Kapre *et al.* [83] reported a room-temperature PVR of 4.5 : 1 in another triple-well/double-barrier structure. Subsequent work by Kapre *et al.* [84] increased the room temperature (77 K) PVR to 4.7 : 1 (7.6 : 1) while maintaining a high current density of 1.25×10^5 A/cm^2. The addition of the InGaAs spacers to structures with hidden ground states (e.g., AlGaAs/InGaAs/GaAs) agrees with the theoretical work of Yoo and co-workers [72] that a reduction of the height in the space-charge barrier that forms in thick spacer layers should improve the PVR.

C. InGaAs/InAlAs/InP

Earlier it was stated that the resonant tunneling current density varies with the electron effective mass with an $\exp(-\sqrt{2m^*})$ dependence. The $In_{0.53}Ga_{0.47}As/In_{0.52}Al_{0.48}As$ system lattice-matched to InP is well known in this regard ($m^* = 0.075m_0$ for an $In_{0.52}Al_{0.48}As$ barrier versus $0.092m_0$ for $Al_{0.33}Ga_{0.67}As$ or $0.15m_0$ for AlAs [85]), so it is a natural candidate for resonant tunneling systems. The first MBE-grown InGaAs/InAlAs/InP RTD was reported in 1986 by Inata and co-workers [85]. The MBE-grown structure consisted of a 61.5-Å InGaAs well, 41-Å InAlAs barriers, and 15-Å undoped InGaAs spacer layers, with both the InGaAs and InAlAs grown at 470°C at a rate of 1.0 μm/h. It exhibited a room-temperature (77-K) PVR of 2.3 : 1 (11.7 : 1), with a 77-K current density of 2.2×10^5 A/cm^2. Subsequent work showed that by reducing the well width, the current density at 77 K could be increased to 5.5×10^5 A/cm^2 [86]. Further reduction of the width of the quantum well width increased the room-temperature PVR to 5.5 : 1 [87].

Potter *et al.* [88] examined InGaAs/InAlAs/InP RTDs with wide (400 Å) undoped InGaAs spacers and reported a room-temperature PVR of 6.7 : 1. Not surprisingly, the peak current density observed with such a wide spacer layer was a relatively low 7.6×10^3 A/cm^2. This structure was grown on an n^+ InP substrate; Potter *et al.* reported that a nominally identical sample grown simultaneously on semi-insulating InP exhibited a

room-temperature PVR of only 5 : 1 and a peak current density of 5.3×10^3 A/cm^2. The inferior structure also exhibited asymmetric I–V characteristics and hysteresis in the NDR region, which was attributed to increased parasitic resistance for structures grown on semi-insulating substrates (rather than temperature, unintentional doping, or other growth-related factors). Oh and co-workers [89] reported a slightly lower room-temperature PVR (6.1 : 1) but a higher peak current (1×10^4 A/cm^2) in a structure with similar barriers and quantum well to those used by Potter *et al.* (45-Å InAlAs and 61-Å InGaAs, respectively) but with very thin (15-Å) undoped InGaAs spacers. Oh *et al.* found a relation between growth temperature and the beam equivalent pressure ratios of arsenic and the group III fluxes, with higher substrate temperatures (e.g., 500 and 525 versus 400°C) and higher P_{As}/P_{III} ratios (e.g., 80 versus 40) yielding higher PVRs. They also reported a high-temperature (800°C) prebake of their 7N indium source in ultrapure hydrogen to reduce residual impurities.

Based on these successes in the growth of InP-based RTD structures, various workers have modified the basic InGaAs/InAlAs system with other materials to enhance its performance. Inata *et al.* [90] replaced the InAlAs lattice-matched barriers with 24-Å pseudomorphic AlAs and observed remarkable PVR values and peak currents: 14 : 1 and 2.3×10^4 A/cm^2 at room temperature and 35 : 1 and 2.3×10^4 A/cm^2 at 77 K. This excellent performance was attributed to a decrease in the valley current (primarily nonresonant thermionic emission) caused by the large AlAs barrier height. Similar characteristics (room-temperature PVR of 24 : 1 and a peak current density of 1.5×10^4 A/cm^2) were obtained in an InGaAs/AlAs pseudomorphic structure on InP by Mehdi and Haddad [92]. The pseudomorphic InGaAs/AlAs structure was further improved by Broekaert *et al.* [93], who substituted six atomic layers of InAs (approximately 18 Å) for InGaAs in the middle of a 35-Å quantum well clad by 28-Å AlAs barriers and 15-Å undoped spacers. The PVRs of this structure (in which the InAs was grown at 420°C while the InGaAs and AlAs were grown at 470°C) were 30 : 1 and 63 : 1 at room temperature and 77 K, respectively; these appear to be the highest peak-to-valley ratios ever reported for a conventional RTD.

To conclude this discussion of InGaAs/InAlAs RTDs it should be noted that lattice-matched growth is not absolutely required; Wolak and coworkers [94] have successfully fabricated $In_{0.2}Ga_{0.8}As/In_{0.2}Al_{0.8}As$ tunneling diodes lattice-mismatched on GaAs. A room-temperature PVR of 4.2 was observed for this structure (compared with a PVR of 3.3 for an identical RTD without indium). Further increases in the In content de-

creased the PVR, presumably due to an increase in misfit dislocations and interfacial roughness.

D. Other Materials

Although "conventional" III–V materials systems such as GaAs/AlGaAs and InGaAs/InAlAs/InP have attracted most of the effort in resonant tunneling structures, some studies have been made of other materials. Inata *et al.* [91] added antimony to AlAs to increase the barrier height and improve the PVR of an InGaAs quantum well structure. They reported a room-temperature PVR of 15 : 1 with a peak current density of 2.4×10^3 A/cm^2 in an RTD with a 44-Å InGaAs well and 29-Å AlAsSb barriers [91]. Beresford and co-workers [95–98] also examined the use of Sb-containing compounds as barriers in resonant tunneling structures. In one study they fabricated an RTD consisting of a 25-Å InAs quantum well, 168-Å AlSb barriers, and 2000-Å InAs contacts on an InAs substrate and observed room-temperature and 77-K PVRs of 1.8 : 1 and 9 : 1, respectively [95]. Growth details (such as doping, substrate temperature, growth rate) were not reported. Note that the small effective mass of electrons in InAs and the large (1.8 eV) conduction band offset with AlSb permitted the use of an extremely wide quantum well.

In a study of structures grown on GaSb substrates, Beresford *et al.* [96] reported NDR in InAs/AlSb RTDs with wells ranging from 150 to 2400 Å. The 77-K PVR for the 1100-Å InAs well was 44 : 1, while the peak current density was a respectable 0.35×10^3 A/cm^2. The resonant tunneling of holes in AlSb/GaSb/AlSb structures grown on GaSb at 485°C has also been reported [98]. An asymmetric structure consisting of a 400-Å InAs well and a single 25-Å AlSb barrier with GaSb cladding exhibited a room-temperature (80-K) PVR of 17 : 1 (80 : 1!) with a low-temperature peak current density of 1.2×10^3 A/cm^2 [97]. Decreasing the InAs well and AlSb barrier thicknesses to 200 and 15 Å, respectively, degraded the PVR slightly [20 : 1 (40 : 1) at 300 K (80 K)] while increasing the room-temperature (80-K) peak current densities to 28×10^3 A/cm^2 (35×10^3 A/cm^2) [97]. Söderström and co-workers [99] decreased the InAs thickness still further (64 Å) and reported a room-temperature peak current density of 3.7×10^5 A/cm^2. Söderström *et al.* [100] have also observed resonant tunneling in a structure consisting of 22-Å $Al_{0.5}In_{0.5}Sb$ barriers and a 110-Å InSb quantum well that was grown at 420°C on GaAs. Although the peak current density was high (3.6×10^4 A/cm^2), the PVRs at room temperature and 77 K were only 1.4 : 1 and 3.9 : 1, respectively.

These low values were attributed to misfit dislocations and microtwins generated at the lattice-mismatched GaAs/InSb heterointerface.

Resonant tunneling diodes based on the MBE-grown NiAl/GaAs epitaxial metal system have been demonstrated by Tabatabaie *et al.* [101]. The structures, which consisted of NiAl quantum wells ranging from 30 to 33 Å thick and 20-Å AlAs barriers, exhibited NDR at room temperature with a PVR of about 2 : 1. The I–V characteristics were highly asymmetric with respect to the origin, suggesting (not surprisingly) that defects were generated at the top NiAl/GaAs interface. Structures fabricated with thicker NiAl quantum wells (50 Å) showed little if any NDR [101].

Finally, it has been demonstrated that suitable tunneling barriers can be fabricated merely through the use of planar doping (also known as δ-doping) [102]. Su and co-workers [103] reported a room-temperature PVR of 1.9 : 1 in a structure in which the "barriers" consisted of the sequence δn^+–15-Å GaAs–δp^+–40-Å GaAs–δp^+–15-Å GaAs–δn^+, where the sheet density of the doped layers was 2×10^{13} cm^{-2} for both δn^+ and δp^+. Subsequent work by Houng *et al.* [104] increased the room-temperature PVR of a structure with δn^+–35-Å GaAs–δp^+–35-Å GaAs–δp^+ barriers to 3.1 : 1 with a high current density of 3 kA/cm^2. They attributed much of this improvement to the use of a relatively low growth temperature of 530°C to minimize dopant diffusion.

IV. MULTIPLE QUANTUM WELL STRUCTURES

The progression from single quantum wells to two or more in a given structure carries a number of interesting applications. Capasso and co-workers [105] have demonstrated that the large difference in the tunneling rates of electrons and holes in a 100-period InGaAs/InAlAs superlattice can result in "effective mass filtering" and lead to large photocurrent amplification. However, extension of the physics of single quantum well phenomena to the sequential resonant tunneling through multiple quantum wells is complicated by the nonuniformity of the electric field in the growth direction and by instabilities arising from negative differential conductivity [106]. The phonon-assisted effective mass filtering examined by Capasso *et al.* and discussed earlier involves hopping conduction between adjacent wells and does not represent a coherent tunneling phenomenon. Summers *et al.* [107] have reported NDR in "energy filters" consisting of two and three quantum wells with varying thicknesses. In order to observe tunneling through coupled quantum wells, very tight control of the thicknesses of the wells and barriers (leading to control of

the energy of the quantized states in the wells) is required; time-resolved photocurrent measurements by Tarucha and Ploog [108] demonstrated that resonant tunneling in coupled quantum wells is significantly disturbed by even monolayer fluctuations in barrier thickness.

Summers *et al.* fabricated a series of two- and three-well structures with 51-Å AlGaAs barriers ($x_{Al} = 0.35$) and 51-Å undoped GaAs spacers. The target well widths ranged from 25.4 to 82 Å; the widths were chosen to be multiples of the monolayer thickness of GaAs to be consistent with layer-by-layer MBE growth. All devices exhibited NDR when forward biased at 77 K, with PVRs found between 5 and 6 : 1. The highly asymmetric *I–V* curves showed the expected absence of NDR under reverse bias.

The *I–V* characteristics of multiple resonant tunneling diodes has been examined by Sen *et al.* [109]. The baseline structure (grown on InP) consisted of a series of 50-Å $In_{0.53}Ga_{0.47}As$ quantum wells clad with 50-Å $In_{0.52}Al_{0.48}As$ barriers and 50-Å undoped $In_{0.53}Ga_{0.47}As$ spacers; each tunneling structure was separated (and electrically connected) via 1000-Å $In_{0.53}Ga_{0.47}As$ layers doped to 5×10^{17} cm^{-3}. Quenching of the resonant tunneling began with the RTD closest to the anode and occurred sequentially with increasing bias, resulting in the appearance of x peaks in the *I–V* curve for x RTDs connected in series. Structures consisting of three and five tunneling structures exhibited PVRs of 5 : 1 at room temperature, while at 77 K the PVR increased to 9 : 1 (three RTDs) and 18 : 1 (5 RTDs). Park and co-workers [110] examined the effect of doping in the intermediate region between the tunnel structures and the effect of individual barrier thickness in multiple AlGaAs/GaAs RTDs and observed peak current densities as high as 2.7×10^4 A/cm^2 and PVRs up to 3.6 : 1.

Sen *et al.* [111] proposed that devices with multiple NDR characteristics could be useful for multiple-valued logic applications such as digital signal processing. Resonant tunneling through coupled quantum wells has other applications; room-temperature oscillations up to 32.6 GHZ have been reported by Tanaka and co-workers [112] in a biwell system consisting of undoped thick (140 Å) and Si-doped thin (51 Å) GaAs quantum wells separated by a 40-Å $Al_{0.3}Ga_{0.7}As$ barrier. In this structure tunneling occurred between the first excited state in the wide well and the ground state in the narrow well. Tunneling in MBE-grown coupled quantum wells has also been used to observe *X*-valley transport in AlAs/GaAs heterostructures [113,114]. Perhaps the most interesting application of multiple quantum wells is the resonant interband tunnel (RIT) diode fabricated by Day and co-workers [115]. In this structure tunneling occurs between the conduction band and valence band on either side of a pair of quantum wells via the confined well states; heavy *n*- and *p*-type doping in the contacts on either sides of the wells populate the states in either well. Day

et al. grew a structure on InP consisting of two 40-Å InGaAs quantum wells separated by a 40-Å InAlAs barrier and confined by InAlAs supply layers that exhibited a PVR of 70 : 1 at room temperature and 125 : 1 when cooled below 200 K. Unfortunately, the peak current density in this structure was very low, partially offsetting the remarkable PVR values.

V. RESONANT TUNNELING TRANSISTORS

A principal long-range application of resonant tunneling structures is their implementation in three-terminal transistors. One approach for achieving this involves combining the NDR behavior of an RTD with the *I–V* characteristics of conventional three-terminal devices to achieve new functions. Note that in this implementation the primary operational parameters of the structure will represent those of the "traditional" device, with the tunneling features added to alter these characteristics. An alternative approach involves the use of tunneling structures without reliance on the principles of operation of conventional transistors.

Several groups have investigated the combined resonant tunneling diodes and field effect transistor structures. In one embodiment, an RTD is substituted for the Schottky barrier gate in a GaAs MESFET [116–118]. This structure represents straightforward sequential MBE growth of a GaAs/AlAs RTD on top of an *n*-GaAs conductive layer. The device operated via modulation of the *I–V* characteristics of the RTD as a function of the source–drain voltage. Note that there were no spacer layers in this structure, indicating a desire for high current at the expense of a large PVR. A combination of an MBE-grown resonant tunneling diode with a quantum well field effect transistor has also been reported by Yang and co-workers [119], while the integration of an RTD with an AlGaAs/GaAs MODFET has been discussed by Longenbach *et al.* [120].

A different approach involves the integration of an RTD as a load element to a MESFET driver [121]. By employing a tunnel diode in place of the conventional depletion mode FET load, the load current is reduced if the RTD is biased off-resonance, thus improving the noise characteristics of the enhancement mode FET. In addition, the nonohmic *I–V* behavior of the RTD led to hysteresis in the FET transfer characteristics; this bistability offers the prospect that the RTD can operate as a memory cell [121]. Again, this structure can be realized by the sequential MBE growth of an RTD on top of an enhancement mode MESFET.

In 1985 Yokoyama and co-workers [122] proposed and demonstrated a resonant tunneling hot electron transistor (RHET) in which an RTD with

50-Å $Al_{0.33}Ga_{0.67}As$ barriers and a 56-Å GaAs quantum well was inserted between the GaAs emitter and base. When the structure was forward biased, electrons were injected into the base by resonant tunneling through the quantum well and subsequently ballistically transferred into the collector. Unfortunately, the device exhibited poor current gains and large base-collector leakage currents [123]. This negative result is not surprising in light of the observations by Capasso and co-workers [124] (who used hot electron transistors with resonant tunneling barriers integrated in the collector) that ballistic electrons are strongly randomized by scattering. However, Seabaugh and co-workers [125] demonstrated room-temperature operation of a RHET that consisted of an AlAs/InGaAs/InAs RTD that served as an injector for an $In_{0.53}Ga_{0.47}As$ base and $In_{0.5}(Al_{0.5}Ga_{0.5})_{0.5}As$ collector. The RTD contained a central 20-Å InAs notch that lowered the base injection energy of the 40-Å well from 0.7 to 0.33 eV. This feature led to room-temperature gain as high as 12 at a current density of 1.3×10^5 A/cm^2.

A number of workers have examined the integration of resonant tunneling structures into heterojunction bipolar transistors (HBTs) as an alternative to hot electron transistors. An early implementation of a resonant tunneling HBT was demonstrated by Capasso *et al.* [126]. This structure consisted of an RTD (74-Å GaAs well, 21.5-Å AlAs barriers) inserted into the HBT base, with the Al mole fraction in the base adjusted to $x_{Al} = 0.07$ so that ΔE_c equaled the first quantized energy level in the quantum well. A current gain of 7 was reported for this device structure. A more complicated resonant tunneling HBT was later reported by Sen *et al.* [127]. This device was fabricated using lattice-matched InGaAs and InAlAs on InP in order to take advantage of the high PVRs of InGaAs/InAlAs/InP double-barrier structures; the specific structure included two RTDs (50-Å quantum wells and 50-Å barriers) embedded in the collector of an InGaAs/InAlAs *npn* transistor (see Fig. 7).

A similar device, consisting of a single RTD in an InGaAs/InAlAs/InP HBT emitter, was demonstrated by Futatsugi *et al.* [123]. This structure was grown at a low substrate temperature (470°C) and consisted of 44-Å InAlAs barriers, 15-Å undoped InGaAs spacers, and a 38-Å InGaAs quantum well. It behaved like a conventional HBT for base currents less than 0.8 mA in the common-emitter configuration; at base currents in excess of 1.0 mA, however, the onset of resonant tunneling led to abrupt changes in the collector current as a function of collector voltage. The room-temperature performance characteristics of this structure (PVR of 3.5 : 1, peak current density of 5.7×10^4 A/cm^2, common-emitter small signal current gain of 24, cutoff frequency of 12.4 GHz) were all superior to those observed in a comparable AlGaAs/GaAs structure [128]. The

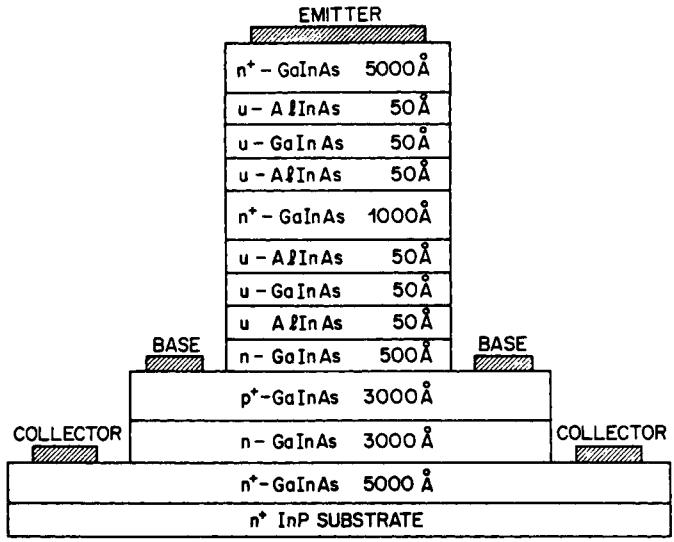

Fig. 7. A resonant tunneling HBT fabricated using lattice-matched InGaAs and InAlAs on InP in order to take advantage of the high PVRs of InGaAs/InAlAs/InP double-barrier structures. (From Ref. 127.)

performance of RTD/HBT hybrids fabricated with AlGaAs/GaAs has been improved; Wu *et al.* [129] reported a room-temperature current gain of 40 with a PVR of 1.9 : 1 when a 50-Å $Al_{0.4}Ga_{0.6}As$/50-Å GaAs RTD was placed between the base and emitter of an HBT. This improvement was attributed to the suppression of both hole diffusion into the double barrier and hole injection from the base into the emitter by the use of a 2000-Å thick n^+-GaAs layer between the RTD and HBT structures.

Although structures that integrate resonant tunneling components into conventional device designs clearly offer performance advantages, the fundamental limitations of the baseline MESFET or HBT will serve to define the ultimate transport and performance characteristics of these devices. Therefore, in order to take advantage of the potential high speed and small size of resonant tunneling structures, it would be desirable to have a "pure" tunneling three-terminal transistor which does not rely on conventional components. This subject has caused significant controversy in the literature concerning the proper definition of a resonant tunneling transistor [130].

Reed and co-workers [131] discussed the fabrication and performance of a three-terminal structure that allowed control of the transfer characteristics via direct manipulation of the energy levels in a quantum well.

This device, termed the bipolar quantum resonant tunneling transistor (BiQuaRTT), consisted of a 150-Å GaAs quantum well, $Al_{0.4}Ga_{0.6}As$ barriers, and emitter and collector regions fabricated from 50-period (80-Å GaAs + 20-Å $Al_{0.4}Ga_{0.6}As$) superlattices (see Fig. 8). The BiQuaRTT was grown at 640°C, except for top (0.5 μm) and bottom (1.5 μm) *n*-GaAs contacts, which were grown at 600°C. The doping deserves special comment: both superlattices were doped with silicon to a nominal level of 2×10^{18} cm^{-3} excluding an undoped spacer of three periods adjacent to the barriers, while the center 50 Å of the quantum well was doped *p*-type with beryllium to 1×10^{19} cm^{-3}. The Be doping was critical to the operation of the device, because it permitted a low-resistance electrical contact to be made to the quantum well via Be ion implantation [132,133]. Because of this contact, negative differential resistance would not be expected; however, negative transconductance, its analog in a three-terminal device, was clearly observed as the common-emitter characteristics I_C versus V_{CE} went through a maximum and then decreased as the voltage on the quantum well base was increased. Before the transconductance went negative, the peak current of the device was 5.6×10^3 cm^{-3}, which was similar to that observed in a control structure grown under the same conditions without a *p*-doped quantum well [131].

Variants on this bipolar resonant tunneling transistor have also been demonstrated. Seabaugh and co-workers [134] described a pseudomorphic version of the BiQuaRTT in which the AlGaAs barriers and superlattice contact were replaced by AlAs barriers and GaAs contacts, respectively. Waho *et al.* [135] fabricated a bipolar transistor in which the

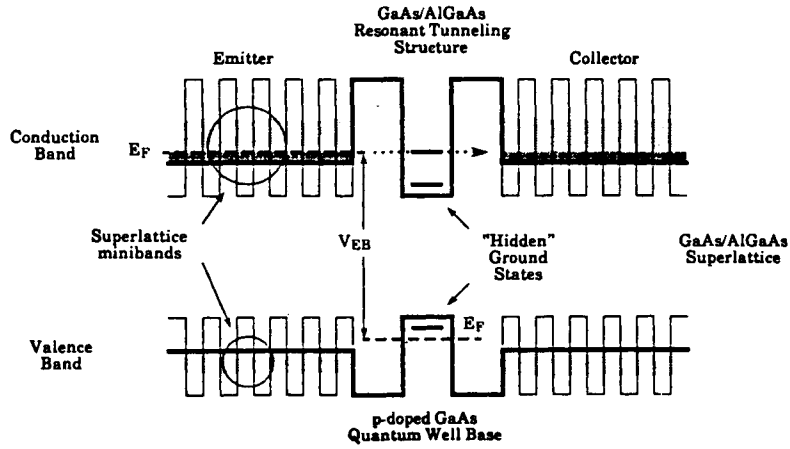

Fig. 8. The bipolar resonant tunneling transistor, developed by Reed *et al.* [131].

base consisted of three 50-Å GaAs quantum wells that were p-doped with Be and separated by 10-Å AlAs barriers. They reported a current gain as high as 5.5 in this device structure.

A unipolar embodiment of a resonant tunneling transistor has been demonstrated by Reddy *et al.* [136]. They grew an 80-Å $In_{0.25}Ga_{0.75}As$ quantum well clad by 40-Å AlAs barriers on top of a 500-Å graded AlGaAs layer ($0.2 \geq x_{Al} \geq 0.1$); the side with the low Al concentration made contact with a 1-μm n^+-GaAs collector. The emitter side of the structure consisted of a 200-Å n^+-GaAs emitter, a 50-Å heavily doped AlAs layer, and finally a 0.3-μm n^+-GaAs emitter contact. The AlAs layer served as an etch stop for fabricating the base contact to the quantum well; Reddy *et al.* [136] stated that surface Fermi pinning completely depleted the 200-Å emitter, thus preventing the base contact from shorting the emitter mesa. Despite the fact that the quantum well was doped to 1×10^{18} cm^{-3}, NDR was observed at room temperature when the device was operated as an RTD, while at 77 K the PVR was about 1.2 : 1. The common-emitter characteristics I_C versus V_{CE} were successfully modulated by the base voltage; however, the gain of the device was low and saturation was never achieved. Following several modifications of this basic MBE-grown structure, Reddy and co-workers [137] were able to achieve a current gain of 3 and a transconductance of 30 mS.

Capasso and co-workers [138] have studied three-terminal structures based on multiple RTDs. In one case, the growth of a conventional RTD (70-Å quantum well clad with 20-Å AlAs barriers) was followed by a modulation-doped heterostructure (200-Å undoped GaAs, 80-Å undoped $Al_{0.35}Ga_{0.65}As$, 400-Å $Al_{0.35}Ga_{0.65}As$ doped with Si to 2×10^{18} cm^{-3}). Subsequent metallization produced two monolithically integrated resonant tunneling diodes, with the modulation-doped layer providing a low-resistance, parallel contact to the tunnel regions beneath the (spatially separated) metallization pads. By altering the bias on the two RTD terminals with respect to the common substrate terminal, multiple resonance peaks were observed in the I–V characteristics, offering the prospect of a three-state memory cell [138]. The parallel connection of monolithically integrated RTDs has also been examined by Yang and Shih [139] in a pseudomorphic 30-Å $Al_{0.4}Ga_{0.6}As$/70-Å $In_{0.2}Ga_{0.8}As$ structure [139].

The unique properties of metal-based resonant tunneling structures has been exploited by Tabatabaie and co-workers [140] to fabricate a three-terminal device. A 33-Å NiAl quantum well clad by 20-Å AlAs barriers was used as the drain electrode in this embodiment; a 0.9-μm doped GaAs cap layer served as the source, while a thick (500 to 800 Å) undoped GaAs layer made contact with one of the AlAs barriers to isolate the n^+-GaAs drain electrode. Negative transconductance was observed in this struc-

ture due to changes in the metallic quantum well energy levels caused by wave function penetration into the gate AlAs barrier as a function of gate-to-drain voltage [140]. This effect was small, however, presumably because of the relatively poor crystalline perfection of the regrown GaAs on top of the metallic quantum well.

ACKNOWLEDGMENTS

I am grateful to G. E. Crook, B. Garni, H. J. Gillespie, E. H. Heller, N. Tabatabaie and T. W. Staley for their for assistance in preparing this chapter and for critical reading and discussions. Special thanks go to B. Garni and E. H. Heller for making their personal libraries of MBE literature available to the author. It is a pleasure to acknowledge the staff of the Wendt Engineering Library at the University of Wisconsin for their help with searching the MBE literature. Preparation of this chapter was supported in part by the National Science Foundation under grant DMR-8907372.

REFERENCES

1. C. T. Foxon and B. A. Joyce, *Curr. Top. Mater. Sci.* **7,** 3 (1981).
2. A. C. Gossard, *Treatise Mater. Sci. Technol.* **24,** 13 (1982).
3. W. T. Tsang, *Semiconductors and Semimetals* **22A,** 95 (1985).
4. M. Pessa, H. Asonen, J. Varrio and A. Salokative, *Phys. Stat. Sol. (a)* **116,** 443 (1989).
5. L. L. Chang and K. Ploog, eds., "Molecular Beam Epitaxy and Heterostructures," NATO ASI Ser., Ser. E, **87.** Martinus Nijhoff, Dordrecht, 1985.
6. E. H. C. Parker, ed., "The Technology and Physics of Molecular Beam Epitaxy." Plenum Publishing, New York, 1985.
7. M. A. Herman and H. Sitter, "Molecular Beam Epitaxy: Fundamentals and Current Status." Springer-Verlag, Berlin, 1989.
8. N. Chand, *J. Cryst. Growth* **97,** 415 (1989).
9. E. G. Scott, S. T. Davey, M. A. G. Halliwell and G. J. Davies, *J. Vac. Sci. Technol. B* **6,** 603 (1988).
10. N. Chand, R. C. Miller, A. M. Sargent, S. K. Sputz, and D. V. Lang, *Appl. Phys. Lett.* **52,** 1721 (1988); N. Chand, A. M. Sargent, J. P. van der Ziel, and D. V. Lang, *J. Vac. Sci. Technol. B* **7,** 399 (1989).
11. H. Asahi, Y. Kawamura, M. Ikeda, and H. Okamoto, *J. Appl. Phys.* **52,** 2852 (1981).
12. N. Pütz, H. Heinecke, M. Heyen, P. Balk, M. Weyers, and H. Lüth, *J. Cryst. Growth* **74,** 292 (1986); T. de Lyon, J. Woodall, M. Goorsky, and P. Kirchner, *Appl. Phys. Lett.* **56,** 1040 (1990).
13. R. Köhrbrück, S. Munnix, D. Bimberg, D. E. Mars, and J. N. Miller, *J. Vac. Sci. Technol. B* **8,** 798 (1990).
14. P. A. Maki, S. C. Palmateer, A. R. Calawa, and B. R. Lee, *J. Vac. Sci. Technol. B* **4,** 564 (1986).
15. C. J. Palmstrom, S. Mounier, T. G. Finstad, and P. F. Miceli, *Appl. Phys. Lett.* **56,** 382 (1990).

16. C. T. Foxon and B. A. Joyce, *Surf. Sci.* **50,** 434 (1975).
17. C. T. Foxon and B. A. Joyce, *Surf. Sci.* **64,** 293 (1977).
18. H. Kunzel and K. Ploog, *Appl. Phys. Lett.* **37,** 416 (1980).
19. J. H. Neave, P. Blood, and B. A. Joyce, *Appl. Phys. Lett.* **36,** 311 (1980).
20. B. J. Wu, Y. J. Mii, M. Chen, K. L. Wang, and J. J. Murray, *J. Cryst. Growth,* **111,** 252 (1991).
21. J. C. Garcia, A. C. Beye, J. P. Contour, G. Neu, J. Massies, and A. Barski, *Appl. Phys. Lett.* **52,** 1596 (1988).
22. R. N. Sacks, D. W. Eichler, R. A. Pastorello, and P. Colombo, *J. Vac. Sci. Technol. B* **8,** 168 (1990).
23. D. L. Miller, S. S. Bose, and G. J. Sullivan, *J. Vac. Sci. Technol. B* **8,** 311 (1990).
24. G. W. Wicks, M. W. Koch, J. A. Varriano, F. G. Johnson, C. R. Wei, H. H. Kim, and P. Colombo, *Appl. Phys. Lett.* **59,** 342 (1991).
25. R. J. Malik, R. N. Nottenberg, E. F. Schubert, J. F. Walker, and R. W. Ryan, *Appl. Phys. Lett.* **53,** 2661 (1988).
26. D. L. Miller, H. T. Yang, and S. W. Zehr, *Proc. SPIE* **323,** 17 (1982).
27. W. D. King, G. J. Griffiths, and S. Giugni, *J. Vac. Sci. Technol. B* **9,** 2771 (1991).
28. R. A. A. Kubiak, E. H. C. Parker, and S. S. Iyer, in "Silicon-Molecular Beam Epitaxy" (E. Kasper and J. C. Bean, eds.). CRC Press, Boca Raton, Florida, 1988.
29. R. J. Malik, *J. Vac. Sci. Technol. B* **5,** 722 (1987).
30. W. T. Tsang, *VLSI Electronics Microstructure Sci.* **21,** 256 (1989).
31. R. J. Matyi, unpublished (1988).
32. A. Ignatiev, *Adv. Mater. Manufac. Proc.* **3,** 599 (1988).
33. A. Ignatiev and C. W. Chu, *Metall. Trans. A* **19,** 2639 (1988).
34. A. Ignatiev, *J. Spacecr. Rockets* **27,** 38 (1990).
35. K. Ploog, *J. Cryst. Growth* **79,** 887 (1986).
36. B. Garni, University of Wisconsin, private communication (1991).
37. A. S. Jordan, *J. Appl. Phys.* **51,** 2218 (1980).
38. D. E. Mars and J. N. Miller, *J. Vac. Sci. Technol. B* **4,** 571 (1986).
39. S. L. Wright, R. F. Marks, and W. I. Wang, *J. Vac. Sci. Technol. B* **4,** 505 (1986).
40. L. P. Ramberg, J. Westin, and T. G. Anderson, *J. Vac. Sci. Technol. B* **5,** 1654 (1987).
41. C. J. Sandroff, F. S. Turco-Sandroff, L. T. Florez, and J. P. Harbison, *Appl. Phys. Lett.* **59,** 1215 (1991).
42. R. Tsu and L. Esaki, *Appl. Phys. Lett.* **22,** 562 (1973).
43. L. L. Chang, L. Esaki, and R. Tsu, *Appl. Phys. Lett.* **24,** 593 (1974).
44. T. C. L. G. Sollner, W. D. Goodhue, P. E. Tannenwald, C. D. Parker, and D. D. Peck, *Appl. Phys. Lett.* **43,** 588 (1983).
45. T. C. L. G. Sollner, P. E. Tannenwald, D. D. Peck, and W. D. Goodhue, *Appl. Phys. Lett.* **45,** 1319 (1984).
46. T. J. Shewchuk, P. C. Chapin, P. D. Coleman, W. Kopp, R. Fisher, and H. Morkoç, *Appl. Phys. Lett.* **46,** 508 (1985).
47. M. Tsuchiya and H. Sakaki, *Appl. Phys. Lett.* **43,** 588 (1986).
48. R. D. Schnell, H. Tews, R. Neumann, A. Mitwalsky, R. Treichler, and G. Packeiser, *Inst. Phys. Conf. Ser.* **106,** 825 (1990).
49. E. X. Ping and H. X. Jiang, *Phys. Rev. B* **40,** 11792 (1989).
50. H. C. Liu and D. D. Coon, *J. Appl. Phys.* **64,** 6785 (1988).
51. H. C. Liu, *J. Appl. Phys.* **67,** 593 (1990).
52. R. Gupta, N. Balkan, B. K. Ridley, and M. Emeny, *Proc. SPIE* ("Physical Concepts of Materials for Novel Optoelectronic Device Applications II: Device Physics and Applications") **1362,** 798 (1990).

53. M. A. Herman, D. Bimberg, and J. Christen, *J. Appl. Phys.* **70,** R1 (1991).
54. R. L. Tober, J. Pamulapati, J. E. Oh, and P. K. Bhattacharya, *Appl. Phys. Lett.* **53,** 883 (1988).
55. J. W. Lee and M. A. Reed, *J. Vac. Sci. Technol. B* **5,** 771 (1987).
56. W. D. Goodhue, T. C. L. G. Sollner, H. Q. Le, E. R. Brown, and B. A. Vojak, *Appl. Phys. Lett.* **49,** 1086 (1986).
57. C. I. Huang, M. J. Paulus, C. A. Bozda, S. C. Dudley, K. R. Evans, C. E. Stutz, R. L. Jones, and M. E. Cheney, *Appl. Phys. Lett.* **51,** 121 (1987).
58. M. A. Reed, J. W. Lee, R. K. Aldert, and A. E. Wetsel, *J. Mater. Res.* **1,** 337 (1986).
59. J. G. Simmons, *J. Appl. Phys.* **34,** 1793 (1963).
60. A. C. Campbell, V. P. Kesan, T. R. Block, G. E. Crook, D. P. Neikirk, and B. G. Streetman, *J. Electron. Mater.* **18,** 585 (1989).
61. J. Söderström and T. G. Anderson, *Superlatt. Microstruct.* **5,** 109 (1989).
62. P. Guéret, C. Rossel, E. Marclay, and H. Meier, *J. Appl. Phys.* **66,** 278 (1989).
63. P. Guéret, C. Rossel, W. Schlup, and H. P. Meier, *J. Appl. Phys.* **66,** 4312 (1989).
64. P. Cheng and J. S. Harris, Jr., *Appl. Phys. Lett.* **56,** 1676 (1990).
65. H. Riechert, D. Bernklau, J. P. Reithmaier, and R. D. Schnell, *Electron. Lett.* **26,** 340 (1990).
66. C. R. Wie and Y. W. Choi, *Appl. Phys. Lett.* **58,** 1077 (1991).
67. M. A. Reed, J. W. Lee, and H. L. Tsai, *Appl. Phys. Lett.* **49,** 158 (1986).
68. M. J. Paulus, E. T. Koenig, B. Jogai, C. I. Huang, C. E. Stutz, and K. R. Evans, *Superlatt. Microstruct.* **7,** 135 (1990).
69. S. Sen, F. Capasso, A. C. Gossard, R. A. Spah, A. L. Hutchinson, and S. N. G. Chu, *Appl. Phys. Lett.* **51,** 1428 (1987).
70. S. Y. Chou and J. S. Harris, Jr., *Appl. Phys. Lett.* **52,** 1422 (1988).
71. S. Muto, T. Inata, H. Ohnishi, N. Yokoyama, and S. Hiyamizu, *Jpn. J. Appl. Phys.* **25,** L577 (1986).
72. H. M. Yoo, S. M. Goodnick, and J. R. Arthur, *Appl. Phys. Lett.* **56,** 84 (1990).
73. I. Mehdi, R. K. Mains, and G. I. Haddad, *Appl. Phys. Lett.* **57,** 899 (1990).
74. C. H. Yang, and R. J. Matyi, *Inst. Phys. Conf. Ser.* **106,** 617 (1990).
75. P. Cheng, and J. S. Harris, Jr., *Appl. Phys. Lett.* **55,** 572 (1989).
76. E. Wolak, E. Özbay, B. G. Park, S. K. Diamond, D. M. Bloom, and J. S. Harris, Jr., *J. Appl. Phys.* **69,** 3345 (1991).
77. H. Toyoshima, Y. Ando, A. Okamoto, and T. Itoh, *Jpn. J. Appl. Phys.* **25,** L786 (1986).
78. M. A. Reed and J. W. Lee, *Appl. Phys. Lett.* **50,** 845 (1987).
79. C. H. Yang and H. D. Shih, *Electron. Lett.* **24,** 554 (1988).
80. J. Söderström, T. G. Anderson, and J. Westin, *Superlatt. Microstruct.* **3,** 283 (1987).
81. R. Kapre, A. Madhukar, K. Kaviani, S. Guha, and K. C. Rajkumar, *Appl. Phys. Lett.* **56,** 922 (1990).
82. I. J. Fritz, P. L. Gourley, and L. R. Dawson, *Appl. Phys. Lett.* **51,** 1004 (1987).
83. R. Kapre, A. Madhukar, and S. Guha, *IEEE Electron Devices Lett.* **11,** 270 (1990).
84. R. Kapre, A. Madhukar, and S. Guha, *Appl. Phys. Lett.* **58,** 2255 (1991); *J. Appl. Phys.* **58,** 2255 (1991).
85. T. Inata, S. Muto, Y. Nakata, T. Fujii, H. Ohnishi, and S. Hiyamizu, *Jpn. J. Appl. Phys.* **25,** L983 (1986).
86. S. Muto, T. Inata, Y. Sugiyama, Y. Nakata, T. Fujii, H. Ohnishi, and S. Hiyamizu, *Jpn. J. Appl. Phys.* **26,** L220 (1987).
87. Y. Sugiyama, T. Inata, S. Muto, Y. Nakata, and S. Hiyamizu, *Appl. Phys. Lett.* **52,** 314 (1988).

88. R. C. Potter, A. A. Lakhani, D. Beyea, and H. Hier, *J. Appl. Phys.* **63,** 5875 (1988).
89. J. E. Oh, I. Mehdi, J. Pamulapati, P. K. Bhattacharya, and G. I. Haddad, *J. Appl. Phys.* **65,** 842 (1989).
90. T. Inata, S. Muto, Y. Nakata, S. Sasa, T. Fujii, and H. Ohnishi, *Jpn. J. Appl. Phys.* **26,** L1332 (1987).
91. T. Inata, S. Muto, Y. Nakata,, and T. Fujii, *Inst. Phys. Conf. Ser.* **106,** 895 (1990); *Jpn. J. Appl. Phys.* **29,** L1382 (1990).
92. I. Mehdi and G. Haddad, *J. Appl. Phys.* **67,** 2643 (1990).
93. T. P. E. Broekaert, W. Lee, and C. G. Fonstad, *Appl. Phys. Lett.* **53,** 1545 (1988).
94. E. Wolak, J. C. Harmand, T. Matsuno, K. Inoue, and T. Narusawa, *Appl. Phys. Lett.* **59,** 111 (1991).
95. L. F. Luo, R. Beresford, and W. I. Wang, *Appl. Phys. Lett.* **53,** 2320 (1988).
96. R. Beresford, L. F. Luo, K. F. Longenbach, and W. I. Wang, *Appl. Phys. Lett.* **56,** 551 (1990).
97. K. F. Longenbach, L. F. Luo, S. Xin, and W. I. Wang, *J. Cryst. Growth* **111,** 651 (1991).
98. R. Beresford, L. F. Luo, and W. I. Wang, *Appl. Phys. Lett.* **55,** 694 (1989).
99. J. Söderström, E. R. Brown, C. D. Parker, L. J. Mahoney, J. Y. Yao, T. G. Anderson, and T. C. McGill, *Appl. Phys. Lett.* **58,** 275 (1991).
100. J. Söderström, J. Y. Yao, and T. G. Anderson, *Appl. Phys. Lett.* **58,** 708 (1991).
101. N. Tabatabaie, T. Sands, J. P. Harbison, H. L. Gilchrist, and V. G. Keramidas, *Appl. Phys. Lett.* **53,** 2528 (1988).
102. K. Ploog, A. Fischer, and E. F. Schubert, *Surf. Sci.* **174,** 120 (1986).
103. Y. K. Su, R. L. Wang, and Y. H. Wang, *Jpn. J. Appl. Phys.* **30,** L292 (1991).
104. M. P. Houng, Y. H. Wang, H. H. Chen, H. C. Wei, and Y. H. Lee, *J. Appl. Phys.* **71,** 780 (1992).
105. F. Capasso, K. Mohammed, A. Y. Cho, R. Hull, and A. L. Hutchinson, *Phys. Rev. Lett.* **55,** 1152 (1985); *Appl. Phys. Lett.* **47,** 420 (1985).
106. F. Capasso, *Semiconductors and Semimetals,* **24,** 319 (1987).
107. C. J. Summers, K. F. Brennan, A. Torabi, and H. M. Harris, *Appl. Phys. Lett.* **52,** 132 (1988).
108. S. Tarucha, and K. Ploog, *Phys. Rev. B* **39,** 5353 (1989).
109. S. Sen, F. Capasso, D. L. Sivco, and A. Y. Cho, *IEEE Electron Devices Lett.* **9,** 402 (1988).
110. B. G. Park, E. Wolak, and J. S. Harris, Jr., *J. Appl. Phys.* **70,** 7141 (1991).
111. S. Sen, F. Capasso, A. Y. Cho, and D. L. Sivco, *IEEE Trans. Electron Devices* **34,** 2185 (1987).
112. Y. Tanaka, H. Kano, M. Hashimoto, and I. Igarashi, *J. Cryst. Growth* **95,** 386 (1989).
113. P. Cheng, B. G. Park, S. D. Kim, and J. S. Harris, Jr., *J. Appl. Phys.* **65,** 5199 (1989).
114. T. Nakagawa, T. Kojima, and K. Ohta, *J. Cryst. Growth* **95,** 357 (1989).
115. D. J. Day, Y. Chung, C. Webb, J. N. Eckstein, J. M. Xu, and M. Sweeny, *Appl. Phys. Lett.* **57,** 1260 (1990).
116. F. Capasso, S. Sen, F. Beltram, and A. Y. Cho, *Electron. Lett.* **23,** 225 (1987).
117. S. Sen, F. Capasso, F. Beltram, and A. Y. Cho, *IEEE Trans. Electron Devices* **34,** 1768 (1987).
118. F. Capasso, S. Sen, and A. Y. Cho, *Appl. Phys. Lett.* **51,** 526 (1987).
119. C. H. Yang, Y. C. Kao, and H. D. Shih, *Appl. Phys. Lett.* **55,** 2742 (1989).
120. K. F. Longenbach, Y. Wang, and W. I. Wang, *Appl. Phys. Lett.* **59,** 967 (1991).
121. K. L. Lear, K. Yoh, and J. S. Harris, Jr., *Inst. Phys. Conf. Ser.* **96,** 593 (1989).

122. N. Yokoyama, K. Imamura, S. Muto, S. Hiyamizu, and H. Nishi, *Jpn. J. Appl. Phys.* **24,** L853 (1985).
123. T. Futatsugi, Y. Yamaguchi, S. Muto, N. Yokoyama, and A. Shibatomi, *J. Appl. Phys.* **65,** 1771 (1989).
124. F. Capasso, S. Sen, A. Y. Cho, and A. L. Hutchinson, *Appl. Phys. Lett.* **50,** 930 (1987).
125. A. C. Seabaugh, Y. C. Kao, J. N. Randall, W. R. Frensley, and M. A. Khatibzadeh, *Jpn. J. Appl. Phys.* **30,** 921 (1991).
126. F. Capasso, S. Sen, A. C. Gossard, A. L. Hutchinson, and J. H. English, *IEEE Electron Devices Lett.* **7,** 573 (1986).
127. S. Sen, F. Capasso, A. Y. Cho, and D. L. Sivco, *Inst. Phys. Conf. Ser.* **96,** 605 (1989).
128. T. Futatsugi, Y. Yamaguchi, K. Ishii, K. Imamura, S. Muto, N. Yokoyama, and A. Shibatomi, *Jpn. J. Appl. Phys.* **26,** L131 (1987).
129. J. S. Wu, C. Y. Chang, C. P. Lee, K. H. Chang, D. G. Liu, and D. C. Liou, *Jpn. J. Appl. Phys.* **30,** L160 (1991).
130. P. H. Singer, *Semicon. Int.* **12**(4), 17 (1989); W. R. Frensley, M. A. Reed, and A. C. Seabaugh, *Phys. Today* **43**(9), 132 (1990); F. Capasso, *Phys. Today* **43**(9), 132 (1990).
131. M. A. Reed, W. R. Frensley, R. J. Matyi, J. N. Randall, and A. C. Seabaugh, *Appl. Phys. Lett.* **54,** 1034 (1989).
132. B. Riccò and P. M. Solomon, *IBM Tech. Disclosure Bull.* **27,** 3053 (1984).
133. R. J. Malik, L. M. Lunardi, J. F. Walker, and R. W. Ryan, *J. Vac. Sci. Technol. B* **6,** 682 (1988).
134. A. C. Seabaugh, W. R. Frensley, J. N. Randall, M. A. Reed, D. L. Farrington, and R. J. Matyi, *IEEE Trans. Electron Devices* **36,** 2328 (1989).
135. T. Waho, K. Maezawa, and T. Mizutani, *Jpn. J. Appl. Phys.* **30,** L2018 (1991).
136. U. K. Reddy, I. Mehdi, R. K. Mains, and G. I. Haddad, *Solid-State Electron.* **32,** 1377 (1989).
137. G. I. Haddad, U. K. Reddy, J. P. Sun, and R. K. Mains, *Superlatt. Microstruct.* **7,** 369 (1990).
138. F. Capasso, S. Sen, A. Y. Cho, and D. L. Sivco, *IEEE Electron Devices Lett.* **8,** 297 (1987).
139. C. H. Yang and H. D. Shih, *Inst. Phys. Conf. Ser.* **96,** 611 (1989).
140. N. Tabatabaie. T. Sands, J. P. Harbison, H. L. Gilchrist, T. L. Cheeks, L. T. Florez, and V. G. Keramidas, *Tech. Dig. Intern. Elect. Dev. Meet.*, Dec. 3–6, 1989, Washington, D.C.